RNA-seq analysis of predictive markers associated with glutamine metabolism in thyroid cancer

YI YOU*, YUHENG ZHOU*, ZILU CHEN, LONGCHENG DENG, YAPING SHEN, QIN WANG, WEI LONG, YAN XIONG, FOXING TAN, HAOLIN DU, YAN YANG, JIANG ZHONG, YUNQIAN GE, YOUCHEN LI and YAN HUANG

Department of Ultrasound, Nanjing Hospital of Chinese Medicine Affiliated to Nanjing University of Chinese Medicine, Nanjing, Jiangsu 210022, P.R. China

Received October 24, 2024; Accepted March 6, 2025

DOI: 10.3892/mmr.2025.13510

Abstract. The incidence of thyroid cancer (TC) increases year by year. It is necessary to construct a prognostic model for risk stratification and management of TC patients. Glutamine metabolism is essential for tumor progression and the tumor microenvironment. The present study aimed to develop a predictive model for TC using a glutamine metabolism gene set. Differentially expressed genes in cells with high glutamine metabolism levels from single cell RNA-sequencing data were compared with genes differentially expressed between normal and TC tissues from The Cancer Genome Atlas Program data. Through Boruta feature selection methods and multivariate Cox regression, six crucial genes were identified for a risk-scoring system to develop a prognostic model. The role of each gene was verified in TC cells *in vitro*. A risk-scoring system was developed according to the glutamine gene set to forecast the overall survival of TC patients. This risk score could stratify TC patients and minimize unnecessary surgeries and invasive treatments. In addition, signal induced proliferation associated 1 like 2 (SIPA1L2), an important gene in the prognostic model, knockdown in TPC-1 and BCPAP cell lines enhanced TC cell proliferation, migration and invasion. A risk model was developed based on a glutamine metabolism gene set. The model has reference values for TC stratification.

Introduction

Thyroid cancer (TC) is the most prevalent endocrine malignant tumor globally, with an annual rise in the incidence of 3% (1-3). It has three main histological types: Differentiated, medullary and undifferentiated, with papillary TC being the most common (4,5). Although papillary TC (PTC) is typically characterized by low malignancy and favorable outcomes the treatment of advanced PTC is difficult, leading to an increase in its mortality rate every year. The prognosis for poorly differentiated TC is extremely poor and a cohort study spanning nearly 20 years (6) indicated that the overall survival (OS) was 4 months, and the disease-specific mortality rate was close to 100%. Therefore, there is a need to discover new biomarkers to diagnose and treat TC in time. These biomarkers are crucial for effective risk stratification, personalized management, minimizing unnecessary surgeries and pinpointing potential therapeutic targets for TC (7,8).

Different types of cancer exhibit an unique tumor microenvironment (TME) (9), where tumor cells repurpose extracellular nutrients into intracellular macromolecules, such as nucleotides and proteins (10) through metabolic reprogramming. Glutamine, widely present in blood and muscles, is extensively consumed by various tumors (11). The proliferation of tumor cells particularly depends on glutamine as the primary energy source for the tricarboxylic acid cycle (12). This supports tumor cell growth and enhances their invasive potential. In addition, glutamine metabolism is crucial in immune reactions and immune functions, making it a promising anti-tumor target (13). In recent years, glutamine and proteins related to glutamine metabolism have shown clear correlations with TC. Yu *et al* (14) found that PTC cells had aberrant overexpression of glutaminase (GLS), which promotes PTC cell growth by stimulating cell proliferation, migration and invasion, while inhibition of GLS activity induced apoptosis and autophagy in PTC cells via the mTORC1 signaling pathway. Zhang *et al* (15) demonstrated that GLS and glutamine dehydrogenase are overexpressed in TC tissues and there is a positive correlation between GLS expression and TNM staging of PTC. Targeting glutamine metabolism with the glutamine metabolism inhibitor 6-diazido-5-oxo-l-norleucine inhibits the proliferation of TC cells and enhances immune response to TC by interfering with the synthesis of proteins and DNA and remodeling the TME.

Advances in single-cell RNA sequencing (scRNA-seq) and data analysis techniques have provided new perspectives

Correspondence to: Professor Yan Huang, Department of Ultrasound, Nanjing Hospital of Chinese Medicine Affiliated to Nanjing University of Chinese Medicine, 157 Daming Road, Qinhuai, Nanjing, Jiangsu 210022, P.R. China
E-mail: jacob6662024@163.com

*Contributed equally

Key words: thyroid cancer, glutamine metabolism, RNA-seq, multivariate Cox regression, Boruta

to uncover molecular features of different cell groups in the TME (16,17). Previous reports note that the scRNA-seq dataset may be an effective method for analyzing gene profiles of immune cells and forecasting the prognosis and immunotherapy response in cancer patients (18,19). The present study analyzed both single-cell and large-scale RNA-seq data from TC patients to identify genes related to glutamine functions in TC. Through these genes, a risk model was developed for TC patients. The results affirmed that this risk model was robust and offered accurate prognostic predictions.

Materials and methods

Acquisition and processing of bulk transcriptome data. All data are available to the public and were primarily sourced from The Cancer Genome Atlas (TCGA, https://portal,gdc.cancer.gov/). TC whole genome-wide expression profiles in transcripts per kilobase per million format, clinical annotations and simple nucleotide variation estimated by VarScan2 Variant Aggregation and Masking tool were retrospectively downloaded utilizing the TCGAbiolinks (version 2.25.0) package (20) from the TCGA database. Samples from TCGA-thyroid carcinoma (THCA; n=572) were included, with 513 TC samples and 59 healthy control samples. The current research respected the data access guidelines of every database. The entire research workflow, including data collection, processing, and analysis, is outlined in Figure 1.

Acquisition and processing of scRNA-seq data. The Gene Expression Omnibus (GEO) database (https://www.ncbi.nlm.nih.gov/geo) contains abundant data from scRNA-seq. A GEO dataset (accession no. GSE184362; https://www.ncbi.nlm.nih.gov/geo/query/acc.cgi?acc=GSE184362), consisting of 7 TC tissue samples was downloaded using scRNA-seq. Through the Seurat package from the R (version 4.2.0; http://www.R-project.org/) (21), the raw data from the dataset were imported as single-cell data. Initially, cells and genes were filtered out based on the following criteria: i) Genes expressed in <1 cell type were removed; ii) cells were deleted where <200 genes were expressed; iii) cells with gene expression between 200-3,000, mitochondrial gene content <20% and unique molecular identifiers of 500 and 12,000 were kept. Data were normalized using the normalizedata function (R Seurat package; version 5.2.1; https://satijalab.org/seurat). Differentially expressed genes (DEGs) in single cells were pinpointed through the connection between average expression and dispersion. Next, principal components analysis was conducted for graph-based clustering. The harmony method was used to eliminate the batch effect of various samples. The FindClusters function (R Seurat package; version 5.2.1) was adopted for shared nearest neighbor modularity optimization according to the clustering algorithm on 22 principal components with 0.2 resolutions, leading to 13 clusters. The RunUMAP function was adopted for Uniform Manifold Approximation and Projection (UMAP). UMAP-1 and UMAP-2 were used to showcase cell groupings. The FindAllMakers function (R Seurat package; version 5.2.1) was used to detect DEGs within cell clusters. Subsequently, cell clusters were distinguished using specific biomarkers for each cell type and the ratio of each cell type was assessed.

Glutamine metabolism-related genes. The AUCell package (version 1.18.0; https://bioconductor.org/packages/release/bioc/html/AUCell.html) (22) was adopted to score pathways for all cells based on gene set enrichment analysis (GSEA). According to the area under the curve (AUC) values of 134 genes related to glutamine metabolism from MSigDB (Table SI), gene expression was ranked for each cell type to determine the proportion of upregulated DEGs in all cells. Higher AUC values were observed in cells that expressed several genes from the gene set. The AUCell_exploreThresholds function (R AUCell package; version 1.18.0) was used to establish the threshold for detecting active cells. Next, the UMAP embedding was used to visualize the active clusters by mapping the AUC value of all cells with the ggplot2 package (version 3.3.5 https://ggplot2.tidyverse.org).

A single-cell pathway in pseudotime. Pseudotime assay was performed based on Monocle 2 (23). To conduct the pseudotime assay on epithelial cells, the initial count data were adjusted by computing size elements for trajectory inference. Genes that were both widely spread out and highly active (empirical dispersion/dispersion fit ≥1 and mean expression ≥0.1) were used to construct the pseudotime trajectory (24). The DDRTree (version 0.1.5; https://CRAN.R-project.org/package=DDRTree) algorithm parameters were initialized with default values. To further examine these diverging occurrences, branched expression analysis modeling was employed within the framework of Monocle2 (version 2; http://cole-trapnell-lab.github.io/monocle-release) to discern all genes with branch-dependent expression (23). A heatmap was plotted using Monocle2 to visualize the branch-dependent expression patterns.

Analysis of cellular communication and levels of ligands and receptors. A cellular communications assay was adopted to evaluate the levels of ligand-receptor pairs in cells and exposed definite pathways (25). CellChat (version 1.1.3; https://github.com/sqjin/CellChat) assay was used to uncover the incoming and outgoing communication patterns of various cell types, measure different pathways of cellular communication and determine the flow of information through signaling pathways or the likelihood of cellular communication (26). CellChat was used to examine the single-cell specimens. Cellular communication in all TC samples was analyzed using CellChat; the processed scRNA-seq information from the Seurat package was imported into CellChat for analysis. The communication signals within TC cells were analyzed to determine the strength of all pathways and identify definite pathways. Default parameters were used in CellChat analyses. $P<0.05$ was considered to indicate a statistically significant difference and the P-value was adjusted using the Benjamini-Hochberg mean.

Gene Ontology (GO) and Kyoto Encyclopedia of Genes and Genomes (KEGG) enrichment analyses. GO (27) analysis was performed to reveal the enriched biological process, molecular function and cellular component. KEGG (28) is a valuable bioinformatics tool used to discern metabolic pathways that are markedly related to the DEGs. The clusterProfiler (version 4.2.2) package (29) was used for GO and KEGG enrichment analyses ($P<0.05$) on glutamine metabolism-related DEGs in TC.

Construction and verification of the risk-scoring system. Prognostic genes were screened among DEGs using Kaplan-Meier (K-M) curves. The genes, meeting P<0.05, were selected for additional examinations. Tumor tissues with clinical information were assigned to a training set (n=348) and a validation set (n=154). Boruta algorithm (R package Boruta; version 8.0.0; https://gitlab.com/mbq/Boruta/) (30) and multivariate Cox regression were then adopted to reduce candidates and develop a risk model. According to the minimum criteria, the penalty parameter (λ) was determined. The risk score was reckoned as follows:

$$\text{riskscore} = \sum_{i=1}^{n} \text{Coef}(\text{gene}_i) * \text{Expression}(\text{gene}_i)$$

(Coef (genei): coefficients, Expression (genei): gene level).

The training cohort was classified into low- and high-risk subgroups. The K-M technique was used to plot survival curves and log-rank tests were conducted to check statistical significance. Receiver operating characteristic (ROC) curves were used to appraise the effectiveness of the prediction model. AUC >0.6 indicated satisfactory prediction performance. During the validation process, the validation cohorts were further categorized into subgroups based on their risk levels and the model accuracy was compared.

Construction and validation of a nomogram. The clinical information (sex, age and tumor stage) of individuals was acquired from the TCGA database. Univariate Cox regression models were employed to analyze these features in conjunction with the risk score. Additionally, a nomogram was developed to forecast OS at 1, 3 and 5 years, with the risk score as a key prognostic indicator. A nomogram was developed by integrating predictive and clinical features utilizing the R package RMS (version 7.0-0; https://hbiostat.org/R/rms/). ROC curves were used to assess the nomogram.

GSEA. GSEA (31) was used to assess whether a predefined geneset exhibited important, consistent variations between two groups. The limma (version 3.50.0) package (32) was applied for gene set variation analysis (GSVA). Gene expression difference between risk cohorts was computed. The clusterProfiler (version 4.2.2) package was applied for GSEA on ranked genes according to log2FC values. For each analysis, gene set permutations were conducted 1,000 times. In the Molecular Signatures Database (MSigDB) Collections, which is A Broad Institute resource for genomics and bioinformatics that organizes annotated gene sets, such as gene sharing functions, locations or regulatory patterns, to support gene expression analysis, pathway studies and omics data interpretation (31,33,34), the gene set was found using c2.cp.kegg.v7.5.1.symbols. Genes with an adjusted P<0.05 were reckoned as prominently enriched.

GSVA. The GSVA (35) package was used to compare the biological function using c2.cp.kegg.v7.5.1.symobols. The pheatmap package (version 1.0.12; https://CRAN.R-project.org/package=pheatmap) was used to show the results.

Immune infiltration analysis. The single-sample GSEA (ssGSEA) (36) is an expansion of GSEA that reckons individual enrichment scores for every combination of a sample and gene set. The ssGSEA result revealed how closely the overall upregulated or downregulated genes were in a definite gene set. A total of 28 immune cells were downloaded from the TISIDB (http://cis.hku.hk/TISIDB/index.php) (37) and their relative enrichment was calculated from all gene expression in tumor samples. Immune cell infiltration between risk cohorts was assessed through the ggplot2 (version 3.3.6) (38) package.

Evaluation of drug sensitivity. The sensitivity of TC patients in two risk subgroups to potential therapeutic drugs was predicted using the oncoPredict (version 0.2) (39) package, based on the IC_{50} from GDSC (https://www.cnacerrxgene.org/) (40) and clinical gene expression.

Somatic mutation analysis. The mutation data illustrated the genomic variations landscape. Different clusters were analyzed using the maftools software (version 2.12.0, https://github.com/PoisonAlien/maftools) for somatic variations, such as tumor mutation burden (TMB) (41). The primary driver genes for tumors were typically those frequently mutated genes with the highest mutation frequency in the top 20 (42).

Cell culture and reverse transcription-quantitative (RT-q) PCR. Normal thyroid cell lines (Nthy-ori3-1) and TC cell lines (TPC-1 and BCPAP) were obtained from the medical research building, Fenglin campus, Fudan University (Jiangsu, China). All cells were verified through Short Tandem Repeat (STR) profiling and all STR identification materials have been placed in the supplementary materials. All cells were cultured in RPMI 1640 medium (cat. no. PM150110; Wuhan Pricella Biotechnology Co., Ltd.) or DMEM (cat. no. ZQ-100; Shanghai Zhongqiao Xinzhou Biotechnology Co., Ltd.) with 10% fetal bovine serum (cat. no. F103-01; Vazyme Biotech Co., Ltd.) and 1% penicillin/streptomycin solution (cat. no. CSP006; Shanghai Zhongqiao Xinzhou Biotechnology Co., Ltd.) at 37˚C with 5% CO_2. RNA was extracted from the cell line using the FastPure Cell/Tissue Total RNA Isolation Kit V2 (cat. no. R223-01; Vazyme Biotechnology). HiScript II qPT SuperMix II reagents were added according to the manufacturer's manual to reverse transcribe RNA into cDNA (cat. no. Q331-01; Vazyme Biotechnology), then the ChamQ SYBR qPCR Master Mix reagent (cat. no. Q331-02; Vazyme Biotechnology) was added. RT-qPCR was performed using a quantitative fluorescence PCR machine (cat. no. ABI 7500; Applied Biosystems; Thermo Fisher Scientific, Inc.). The thermocycling protocol used was as follows: 95˚C for 30 sec; followed by 40 cycles of 95˚C for 10 sec, 60˚C for 30 sec, 95˚C for 15 sec, 60˚C for 60 sec and 95˚C for 15 sec. After obtaining the CT values, comparisons between multiple groups were made using the $2^{-\Delta\Delta Cq}$ method (43). All experiments were repeated three times. The primer sequences are shown in Table SII.

RNA interference. SIPA1L2 small interfering RNA (siRNA) was designed and synthesized by Generay Biotech Co., Ltd (Table SII). The logarithmic-phase TPC-1 and BCPAP cells were digested with trypsin for 2 min at 37˚C, and the resulting cell suspension was resuspended in antibiotic-free medium and seeded into a 6-well plate at a density of $8x10^5$ cells per well. When the cell density reached ~70%, the Hieff Trans®

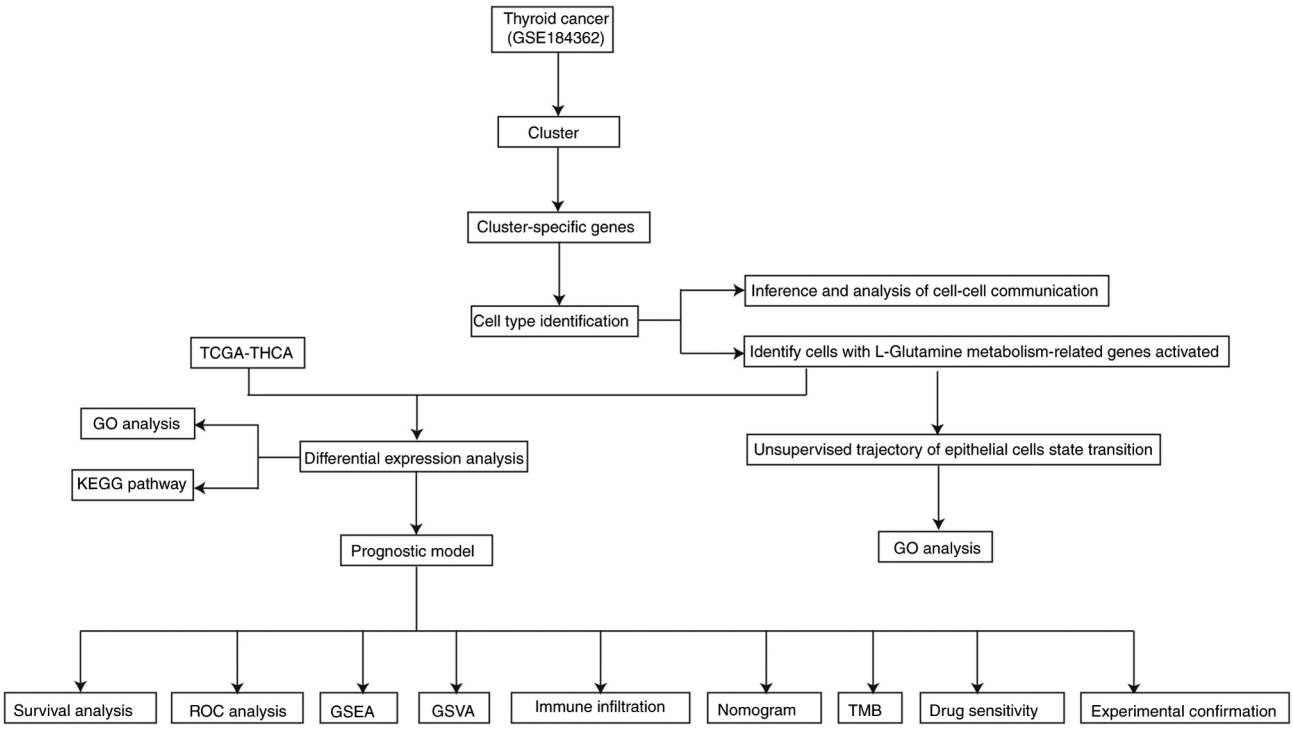

Figure 1. Flowsheet of the entire study. TCGA, The Cancer Genome Atlas; THCA, thyroid carcinoma; GO, Gene Ontology; KEGG, Kyoto Encyclopedia of Genes and Genomes; ROC, Receiver operating characteristic; GSEA, gene set enrichment analysis; GSVA, gene set variation analysis; TMB, tumor mutation burden.

liposomal transfection reagent (cat. no. 40802ES03; Shanghai Yesen Biotechnology Co., Ltd.) and RNAi complexes were added for transfection. The procedure involved mixing 5 μl of transfection reagent with 250 μl of serum-free medium or combining 100 pmol RNAi with 250 μl of serum-free medium, then combining these solutions and incubating at room temperature for 20 min. The mixture was then added to the cells, and the cells were incubated at 37˚C with 5% CO_2 for 24 h to complete the transfection.

5-Ethynyl-2'-deoxyuridine (EdU) staining.The transfected cells were resuspended and seeded in a 12-well plate with coverslips (3x10^5 cells/well). After incubating at 37˚C with 5% CO_2 for 24 h, the EdU probe (cat. no. C0071S; Beyotime Institute of Biotechnology) was added and cells were incubated at 37˚C for 2 h. The cells were then fixed at room temperature with 4% paraformaldehyde for 15 min, permeabilized with 0.5% Triton-X-100 at room temperature for 15 min, stained with Azide 488 at room temperature in the dark for 1 h and subsequently stained with Hoechst 33342 at room temperature in the dark for 30 min. Cell proliferation was observed using a fluorescence microscope (Olympus BX43; Olympus Corportation) using a x10 objective. The coverslip was divided into four areas: Upper left, lower left, upper right and lower right, and images were captured from these fields.

Healing assay. Transfected cells were resuspended and cultured in a 12-well plate. After 24 h, when cells reached 95% confluence, a cross-shaped scratch was created using a sterile 200 μl pipette tip. After PBS washing, the cells were cultured in a serum-free medium and photographed at 0 and 24 h.

Transwell assay. Transfected cells were resuspended in a serum-free medium at 2x10^5 cells per well. The upper chamber was pre-coated with Matrigel solution (Beyotime Institute of Biotechnology) at 37˚C for 3 h. Subsequently, 200 μl of the cell suspension was added in the upper chamber and 600 μl of complete medium was added in the lower chamber. The cells were incubated at 37˚C for 24 h. After 24 h, the cells were fixed with 4% paraformaldehyde at room temperature for 30 min and stained with 0.1% crystal violet (Beyotime Institute of Biotechnology) at room temperature for 30 min. Samples were removed from the chamber, placed on a slide and observed using an inverted DMI3000B fluorescence microscope (Leica Microsystems GmbH) with a x10 objective to assess cell invasion. The chamber was divided into four areas: Upper left, lower left, upper right, and lower right, and images were taken from these fields.

Statistical analysis. R (version 4.1.2; http://www.R-project.org/) was applied for data analysis and statistical calculations. K-M curves and log-rank tests were adopted for survival analysis. Prognostic variables were assessed using Cox regression analysis. Factors with a greater impact on results were identified using the Boruta algorithm. R program ggplot2 was used to visualize the data and the R survival package was used to calculate OS and risk scores. Significant quantitative differences in variables with normal distribution were analyzed utilizing two-tailed t-tests or one-way ANOVA, with Tukey's correction for multiple comparisons. Wilcoxon and Kruskal-Wallis tests were adopted to assess notable variances in data without normal distribution. $P<0.05$ was considered to indicate a statistically significant difference.

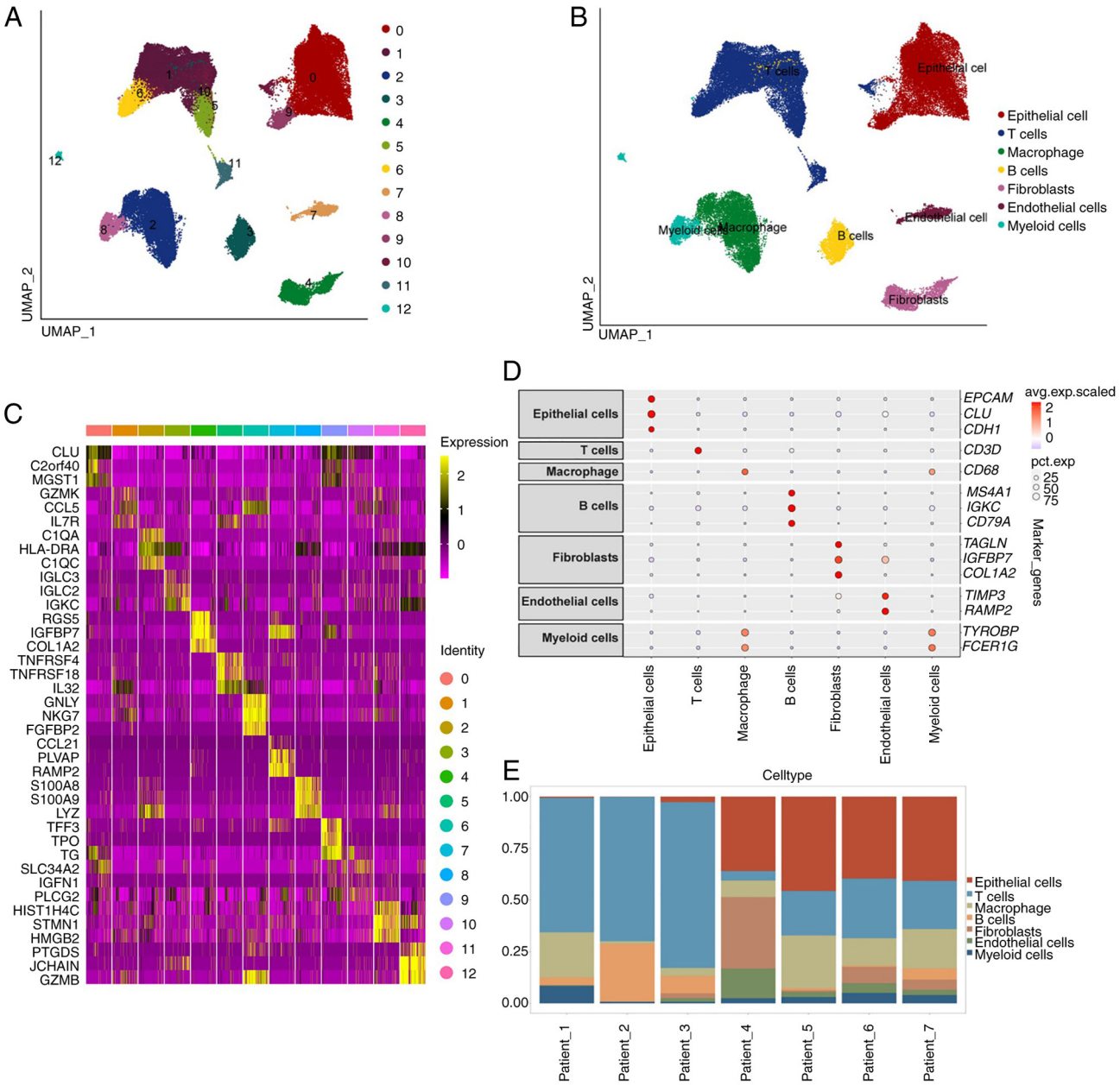

Figure 2. ScRNA-seq data recognize cell subgroups and marker genes. (A) UMAP displays TC cell distribution. (B) UMAP reveals annotation outcomes of TC cell subgroups. (C) Heatmap reveals the specific genes of cell subgroups. (D) Key gene expression in all cell types. (E) Cumulative histogram of the distribution of each cell type in 7 samples. scRNA-seq, single-cell RNA sequencing; UMAP, Uniform Manifold Approximation and Projection; TC, thyroid cancer.

Results

ScRNA-seq analysis. Cell populations of TC were examined to investigate highly expressed genes using the GSE184362 dataset. After an initial evaluation of quality control and removal of duplicates, single-cell transcriptomes of 56,580 cells were obtained. All cells were clustered into 13 distinct groups (Fig. 2A). Distinct cell types were discovered based on the genetic features of each group using cell type-specific biomarkers listed in Table SIII. A total of seven cell types, containing epithelial cells, macrophages and T cells are displayed in Fig. 2B. Marker gene levels of all groups are shown in the heatmap (Fig. 2C). Distinct genes associated with individual cell types are visualized in dot plots (Fig. 2D). The distribution of cell types in all samples is shown in Fig. 2E.

Identification of glutamine metabolism-related active cells. To explore the primary sites of glutamine metabolism in TC, the present study identified active cell subpopulations at the single-cell level using the expression patterns of glutamine metabolism-related genes. Active cells were determined by the optimal threshold, with cell populations having an AUC value >0.12 considered as high glutamine metabolism activity groups and those with an AUC value <0.12 as low glutamine metabolism activity groups. The results showed that there were 1,751 glutamine metabolism -active cells (Fig. 3A). The AUCell scores of glutamine metabolism for each cell type was further calculated and their differences before and after the occurrence of TC compared. Fig. 3B displays the t-SNE plot of active cells, where epithelial cells showed the highest glutamine metabolism scores among all cells, thus the present study

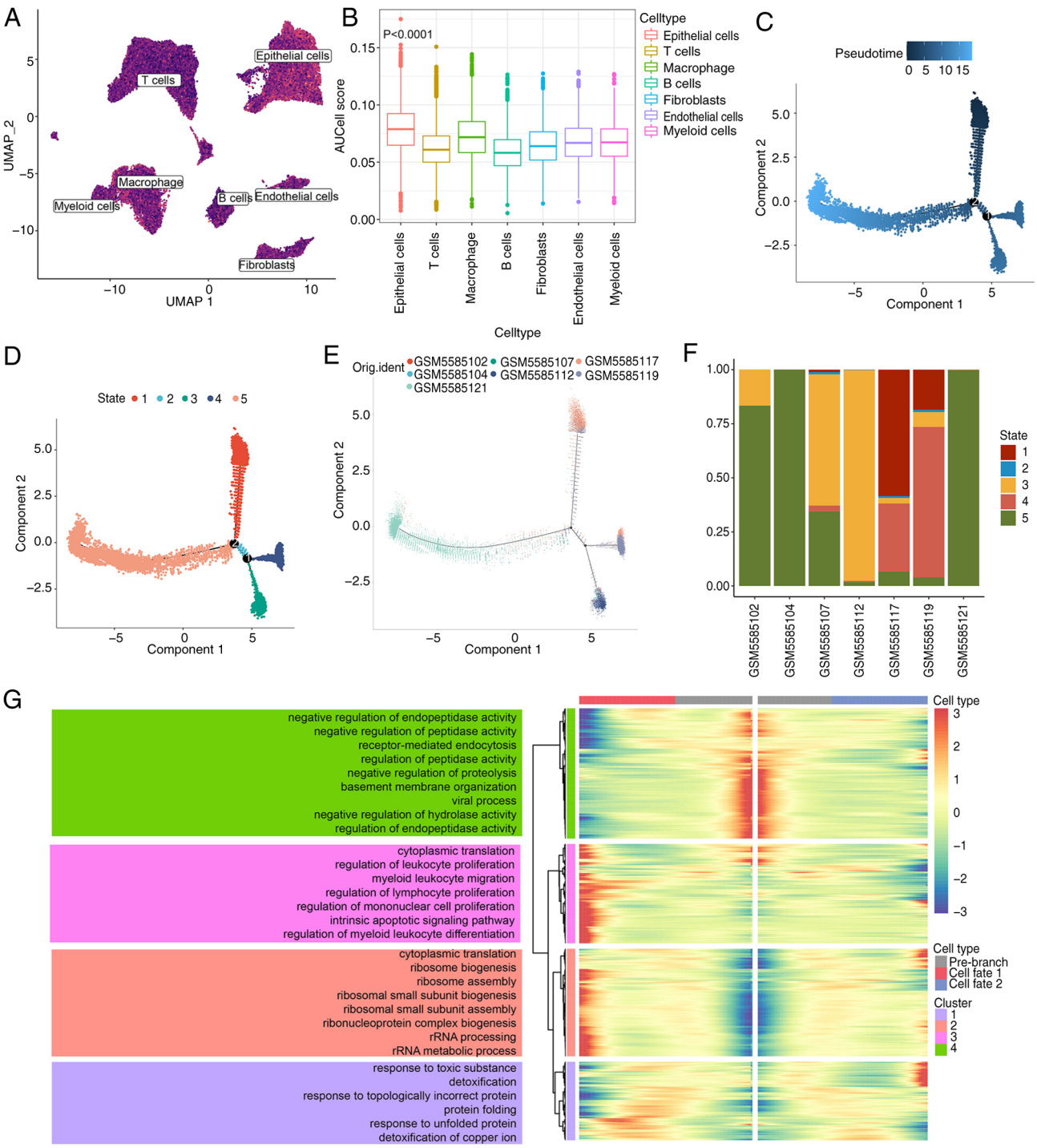

Figure 3. Identification of active cells in glutamine metabolism and pseudotime analysis in TC (A) UMAP colorogram displays cell activity. The brighter color denotes the higher activity score. (B) The AUCell score of cell types. (C) The pseudotime color from dark to light blue. (D) The pseudotime trajectory is separated into five states by Monocles2. (E) Pseudotime trajectory displays the spread of cells from TC based on the samples. (F) A cumulative histogram demonstrates cell states in samples. (G) DEGs of various branches in a heatmap with the top GO BP pathways itemized nearly. TC, thyroid cancer; UMAP, Uniform Manifold Approximation and Projection; DEGs, differentially expressed genes; GO BP, Gene Ontology Biological Process.

regarded them as the main subjects for subsequent analysis. A transcriptional trajectory was constructed using definitive epithelial cells to identify crucial gene expression patterns that govern TC progression. Differentiated paths were revealed in the trajectory's transcriptional states. Epithelial cells showed five states, in which epithelial cells from the GSM5585102, GSM5585104 and GSM5585121 datasets were enriched in state 5 and the remaining epithelial cells were enriched in states 1-4 (Fig. 3C-F). The genes responsible for the first branching point of TC were investigated to understand the molecular basis. Highly expressed genes in pre-branch cells were mainly enriched in pathways related to inhibiting endopeptidase activity, peptidase activity and receptor-mediated endocytosis. In addition, genes enriched in cytoplasmic translation, adjustment of leukocyte proliferation and myeloid leukocyte migration showed high expression in cell fate 1 (Fig. 3G).

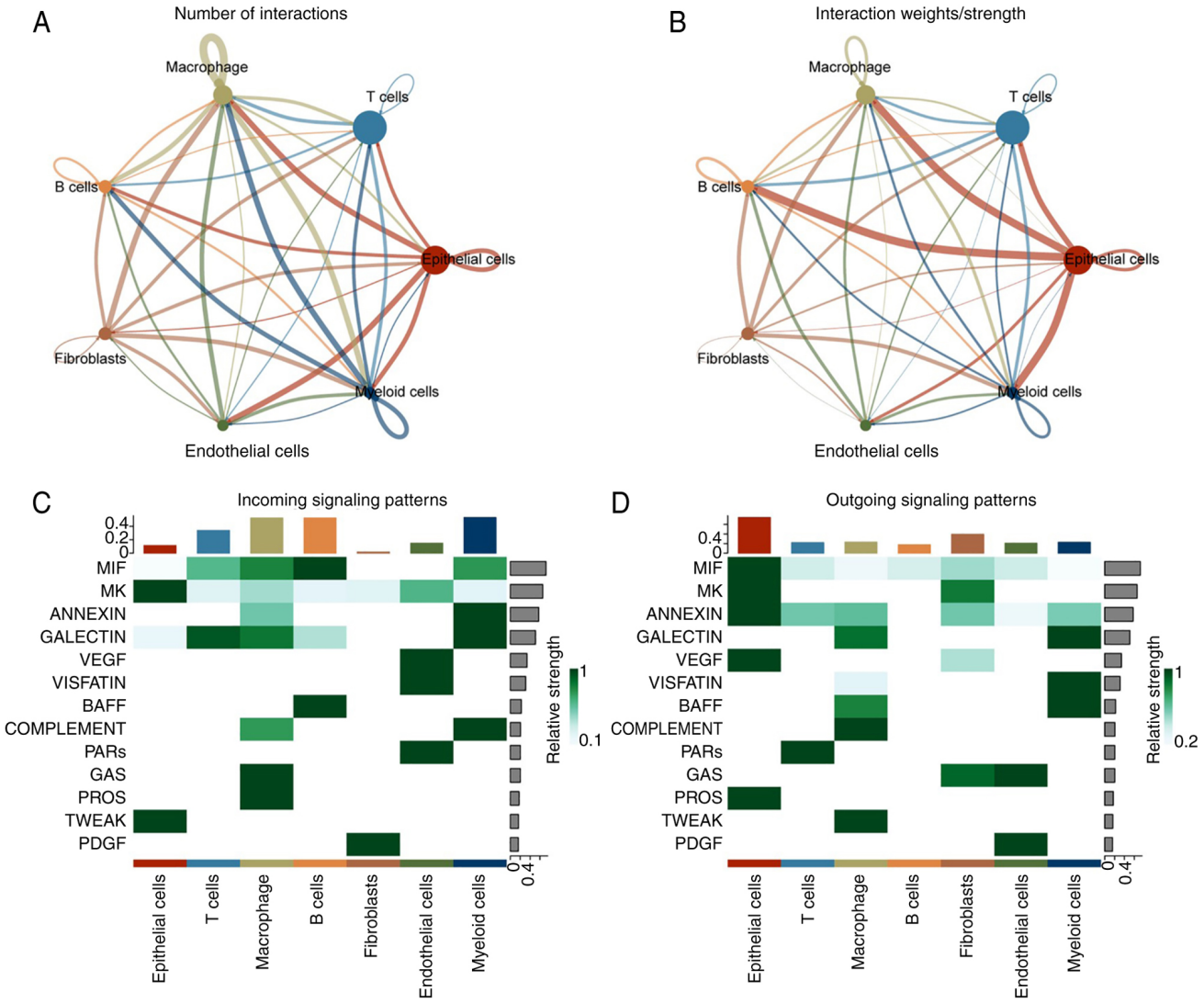

Figure 4. Cell communication analysis in TC (A) Cell interaction quantity. (B) Cell interaction intensity. (C) Heatmap displaying the probable incoming signaling pathways. (D) Heatmap showing the potential outgoing signaling pathways. TC, thyroid cancer.

Cellular communication in the TC TME. The interactions between these types of cells are shown in Fig. 4A and B. Subsequently, the potential signals and specific pairs of molecules in these seven types of cells were analyzed. Macrophages were the primary source of signals, while epithelial cells were the main recipients (Fig. 4C and D). Epithelial cells potentially communicated through the MK, TWEAK, MIF, ANNEXIN and VEGF signaling pathways. Consequently, the specific signal pairs in epithelial cells were examined. The findings indicated that epithelial cells primarily communicated with B cells through the MIF-(CD74+CXCR4) signaling pathway, while fibroblasts communicated with themselves through the MDK-SDC4 and MDK-NCL signaling pathways (Fig. S1A-C). The ligand MIF was primarily expressed in epithelial cells (Fig. S1D). CD74 and CXCR4 receptors were expressed in B cells. The ligand MDK was primarily expressed in epithelial cells and fibroblasts (Fig. S1E). SDC2 and SDC4 receptors were mostly expressed in epithelial cells. NCL receptor was expressed in various cells.

Analysis of gene enrichment in TC focusing on DEGs associated with glutamine metabolism. A total of 2,098 DEGs were uncovered between epithelial cells and other cell types, with P<0.05 and |Log2 fold change|>0.25 (Table SIV and Fig. 5A). A total of 5,825 DEGs were found between TC issues and control thyroid issues (P<0.05, |Log2 fold change|>0.5). The top 10 upregulated and downregulated genes in TC samples are displayed in a heatmap (Table SV, Fig. 5B). The intersection between the two types of DEGs yielded 633 hub genes (Table SVI; Fig. 5C). To explore the biological roles of the central genes, the GO (Table SVII) and KEGG analyses (Table SVIII) were conducted. These genes were enriched in pathways linked to T cell (GO: 0042110), lymphocyte activation (GO: 0051251) and cell adhesion (GO: 0045785; Fig. 5D). The enhanced KEGG pathways comprised the synthesis of thyroid hormone (hsa04918), infection by human T-cell leukemia (hsa05166) and Epstein-Barr virus (hsa05169; Fig. 5E).

Establishment and verification of a prognostic risk model. DEGs in epithelial cells were compared with those in TC and control groups. Signature genes in epithelial cells were distinguished utilizing the K-M curve with P<0.05. In Table SIX, 63 TC-associated genes were ultimately pinpointed. Boruta

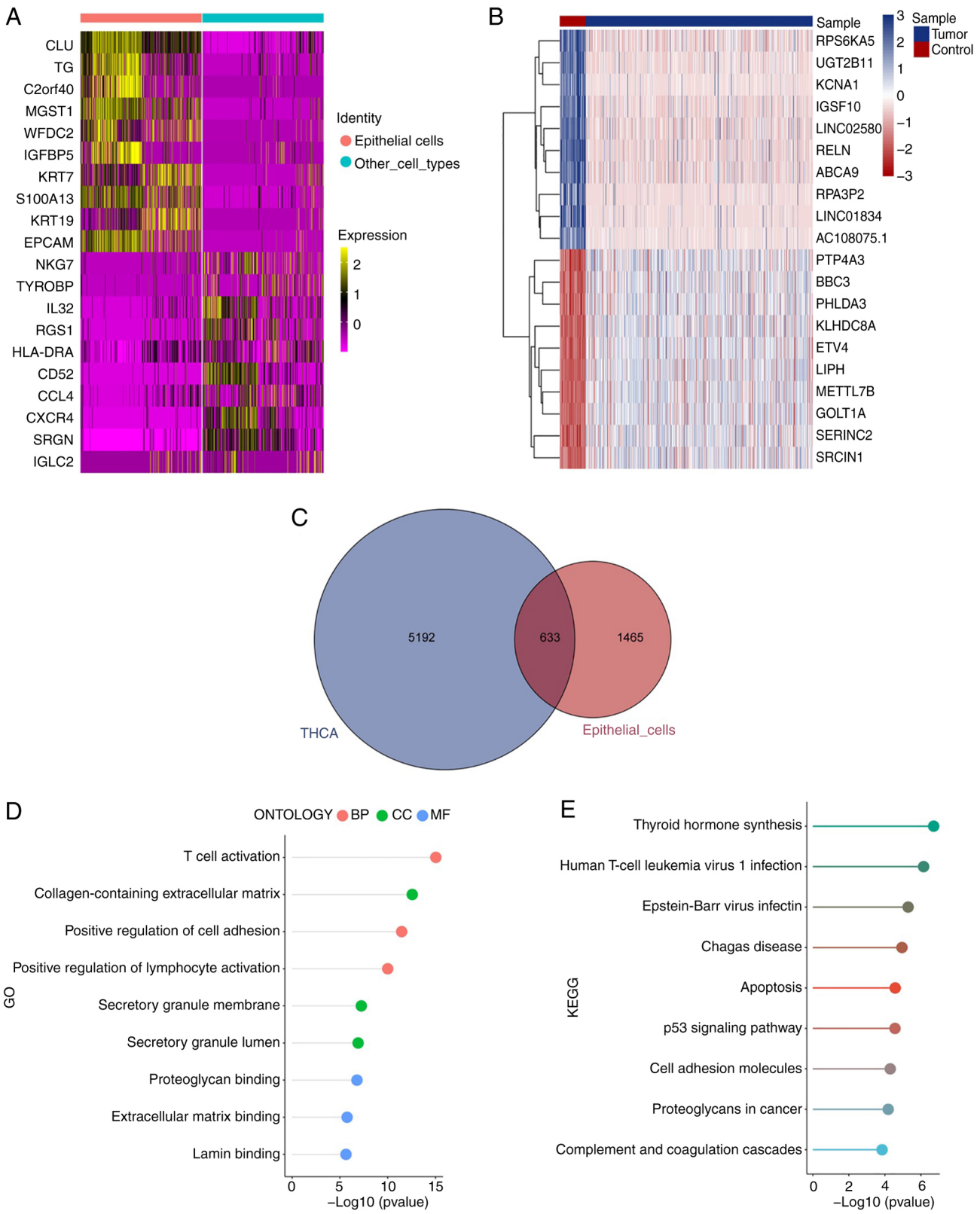

Figure 5. Enrichment analysis of DEGs associated with glutamine metabolism in TC. (A) DEGs in epithelial cells of TC. (B) The top 20 DEGs in TC. (C) Venn diagram of hub genes. (D) GO analysis. (E) KEGG analysis. DEGs, differentially expressed genes; TC, thyroid cancer; GO, Gene Ontology; KEGG, Kyoto Encyclopedia of Genes and Genomes.

was further screened among 63 targets and 17 genes were obtained. The model was constructed by multivariate COX and the genes with a linear relationship with each other were removed by collinearity analysis and six genes were obtained after optimizing the model, with the seed value set to 78. A total of six genes (S100A13, APOE, TUSC3, SNX22, SIPA1L2 and PSMB8) associated with TC prognosis were discovered. 70% of TC samples (n=502) were chosen for the training set

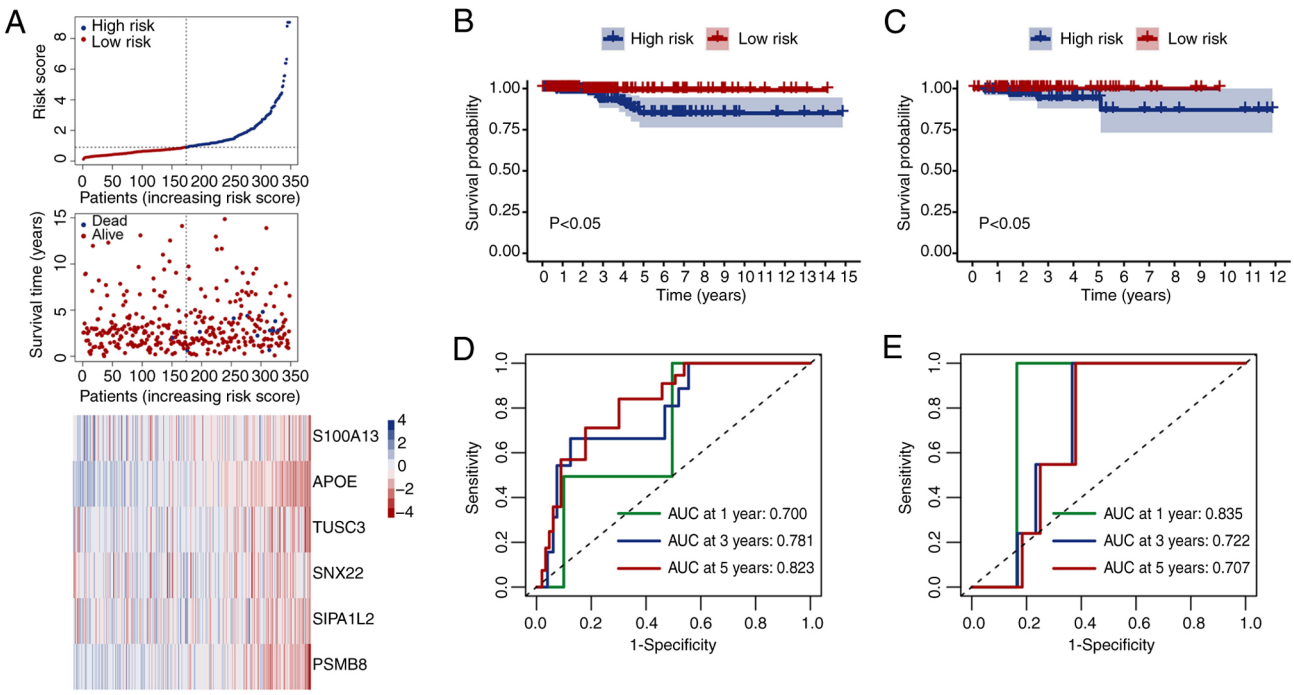

Figure 6. Cox regression analysis and feature selection of the TC dataset. (A) Risk score distribution, survival outline and heatmap of hub genes in the training cohort. (B) Survival curve in the training set. (C) Survival curve in the validation set. Blue represents high-risk cohorts and red represents low-risk cohorts. (D) ROC curves for 1-, 3- and 5-year survival in the training set. (E) ROC curves for the validation set. TC, Thyroid cancer; ROC, Receiver Operating Characteristic.

(n=348), while 30% of samples were allocated to the validation set (n=154). The model constructed based on these six genes was evaluated by dividing the samples into high- and low-risk categories according to the median score. Risk scores, survival time and levels of six genes in various groups from the training set are displayed in Fig. 6A. The high-risk population exhibited a greater density of death states and increased gene levels. Survival curves were generated for patients in various groups in the training (Fig. 6B) and validation sets (Fig. 6C). High-risk populations had notably worse prognoses than low-risk populations across all cohorts. The effectiveness of the model in forecasting patient outcomes was assessed using ROC curves. The training set showed 0.7, 0.781 and 0.823 AUC values for 1-, 3- and 5-year survival rates, respectively (Fig. 6D). The validation cohort showed AUC values of 0.835, 0.722 and 0.707, respectively (Fig. 6E). To explore the mechanisms underlying these DEGs, GSEA using MSigDB Collection identified that LYSINE_DEGRADATION, PROPANOATE_METABOLISM and ASCORBATE_AND_ALDARATE_METABOLISM were enriched in the high-risk cohorts, while TYPE_I_DIABETES_MELLITUS, ALLOGRAFT_REJECTION and SYSTEMIC_LUPUS_ERYTHEMATOSUS were enriched in the low-risk cohorts (Fig. S2A-F; Table SX). Additionally, GSVA highlighted five pathways with the most notable differences between the high-risk and low-risk populations (Fig. S2G; Table SXI).

Immune infiltration analysis. The infiltration of 28 immune cells was evaluated by the ssGSEA technique (Table SXII). The proportions of 28 cells were manifested in a stacked bar plot (Fig. 7A). In addition, cell division differed among TC patients. Most immune cells showed positive correlations with others (Fig. 7B). Monocytes were negatively linked with myeloid-derived suppressor cells (Fig. 7B). Noticeable differences were observed between the high-risk and low-risk populations in Activated B cell, Activated CD4 T cell and Activated CD8 T cell (P<0.05; Fig. 7C).

Construction and verification of nomogram. To verify whether the risk score can serve as an independent prognostic factor, univariate Cox regression analysis was performed on the patients' clinical characteristics, such as age, stage and sex. All clinical data were sourced from the TCGA database. The results of the univariate Cox regression analysis indicated that stage, age and risk score were all associated with the patients' prognostic risk (Fig. 8A). Based on the prognostic risk factors obtained from the R package RMS and one-way COX, the present study constructed a nomogram of prognostic diagnosis (Fig. 8D) and detected its diagnostic value by ROC curve and calibration curve. AUC values for survival rates at 1, 3 and 5 years were 0.979, 0.941 and 0.939, respectively (Fig. 8B). The results indicated that the prognostic model had good diagnostic value for the prognosis of patients. The calibration curve also shows minimal deviation from the ideal model, suggesting good predictive performance of the model (Fig. 8C).

TMB and drug susceptibility analysis. The specific genetic mutation in TC was evaluated and the top 20 driver genes with frequent mutations were screened. BRAF was the most frequent mutation, followed by NRAS (Fig. 9A and B). TMB is a vital element in determining response to immunotherapy. Consequently, genetic mutations related to TC were examined. The high-risk population displayed markedly greater TMB than the low-risk population (P<0.05; Fig. 9C). The present study focused on determining the effectiveness of risk scores in predicting chemotherapy response

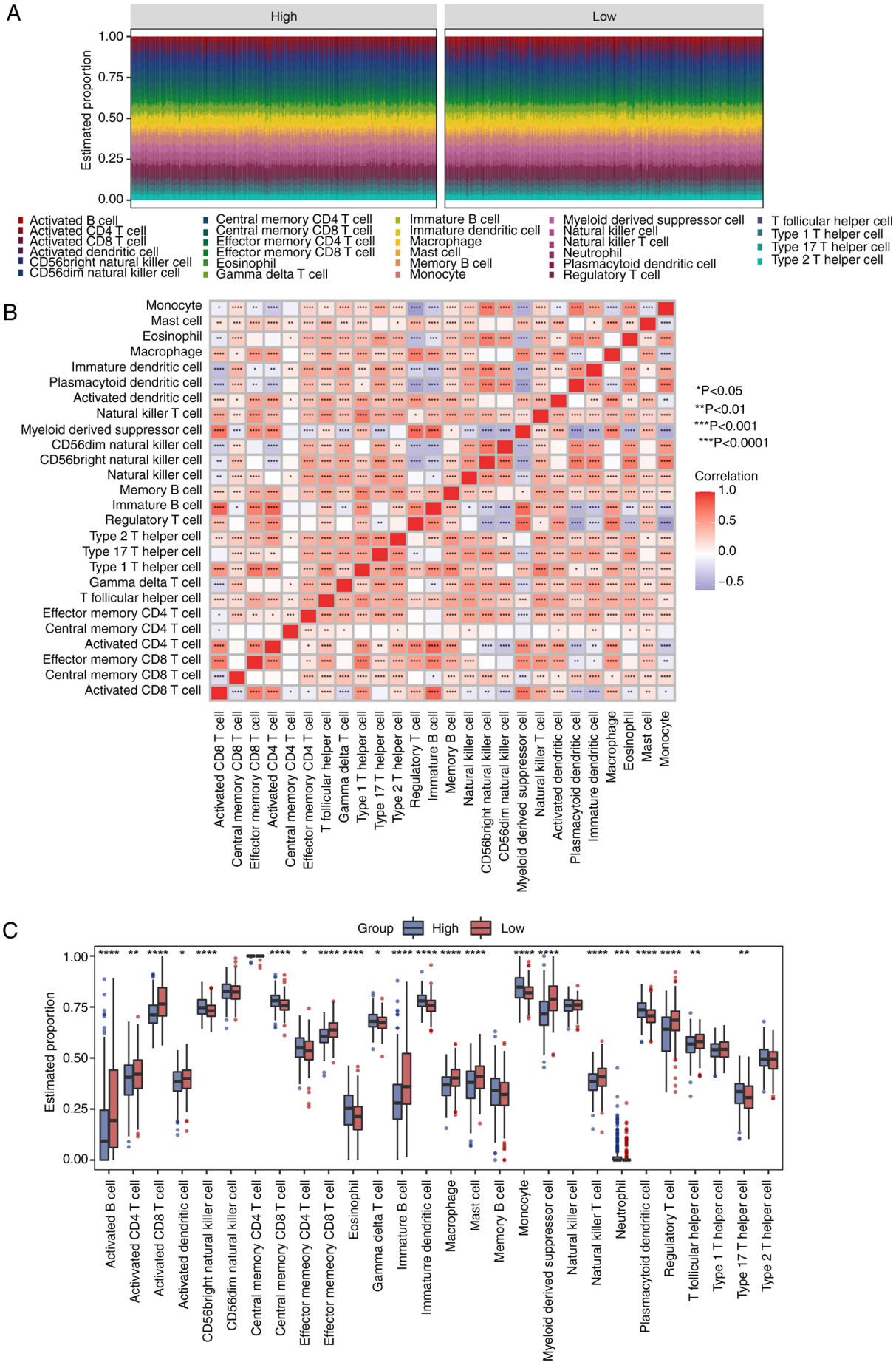

Figure 7. Immune infiltration analysis between TC and control. (A) Immune infiltration in TC. (B) Relevance of immune cells (****P<0.0001, ***P<0.001, **P<0.01 and *P<0.05). (C) Estimated proportions of immune cells among two groups. TC, thyroid cancer.

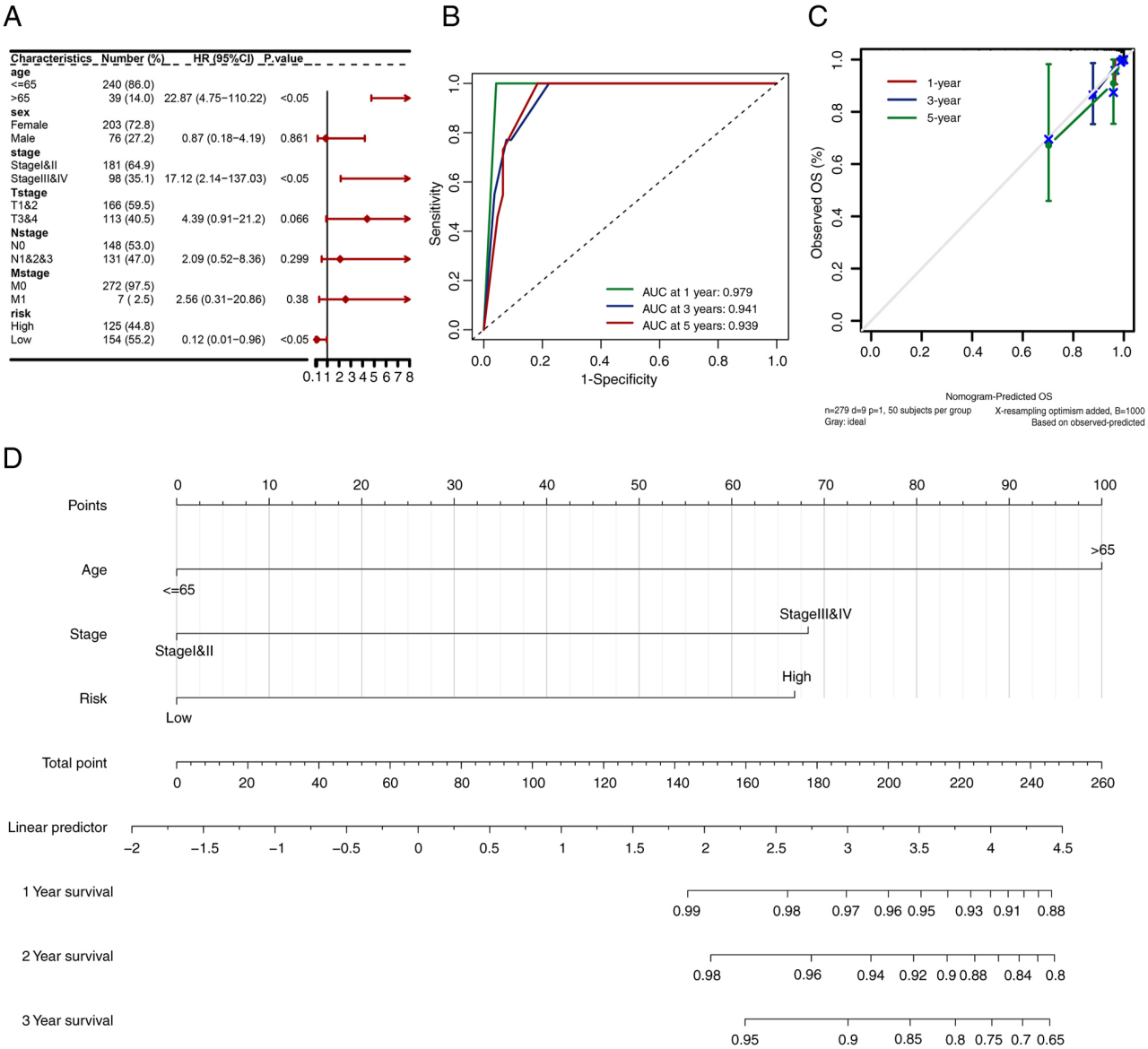

Figure 8. Construction and validation of prognostic models based on prognostic genes (A) Forest map displaying the univariate Cox regression based on clinical features. (B) ROC curves for 1-, 3- and 5-year survival of the nomogram. (C) Calibration curves for 1-, 3- and 5-year survival of the nomogram. (D) The prediction nomogram. The line segment shows the contribution of the clinical element to survival, total points are the total score of all variables and the bottom lines show 1-, 3- and 5-year survival, respectively. ROC, receiver operating characteristic.

in TC patients. Camptothecin_1003, Dactinomycin_1811, Dactinomycin_1911, Dactolisib_1057, Epirubicin_1511, MG-132_1862, Podophyllotoxin bromide_1825 and Sabutoclax_1849 were investigated for the clinical efficiency of TC treatment (Table SXIII). Low-risk patients may exhibit high sensitivity to Camptothecin_1003 (Fig. 9D), Dactinomycin_1811 (Fig. 9E), Dactinomycin_1911 (Fig. 9F), Dactolisib_1057 (Fig. 9G), Epirubicin_1511 (Fig. 9H), MG-132_1862 (Fig. 9I), Podophyllotoxin bromide_1825 (Fig. 9J) and Sabutoclax_1849 (Fig. 9K). These results suggest that chemotherapy could be a favorable option for low-risk individuals.

Validation of levels of six genes in TC cell lines. The mRNA levels of S100A13, APOE, TUSC3, SNX22, SIPA1L2 and PSMB8 differ between normal thyroid cells (Nthy-ori3-1) and TC cell lines (TPC-1, BCPAP). S100A13, APOE, TUSC3, SNX22 and SIPA1L2 have higher mRNA expression levels in the BCPAP cell line compared to normal thyroid cells, while APOE, TUSC3, SNX22 and SIPA1L2 have higher expression levels in the TPC-1 cell line compared to normal thyroid cells. However, the expression level changes of S100A13 and PSMB8 in the TPC-1 cell line were not statistically significant (Fig. 10A).

Validation of SIPA1L2 in vitro. Existing literature reports that the TUSC3 and APOE genes play a role in promoting disease progression in TC (44,45). The present study found that the changes in mRNA expression levels of PSMB8 and S100A13 genes in TPC-1 cells were not statistically significant. SNX22 itself is expressed at low levels in TC and is not easily knocked down. Therefore, the present study chose to validate the role of the SIPA1L2 gene in TC cells. After knocking down the SIPA1L2 gene, mRNA level detection revealed that it could be knocked down by more

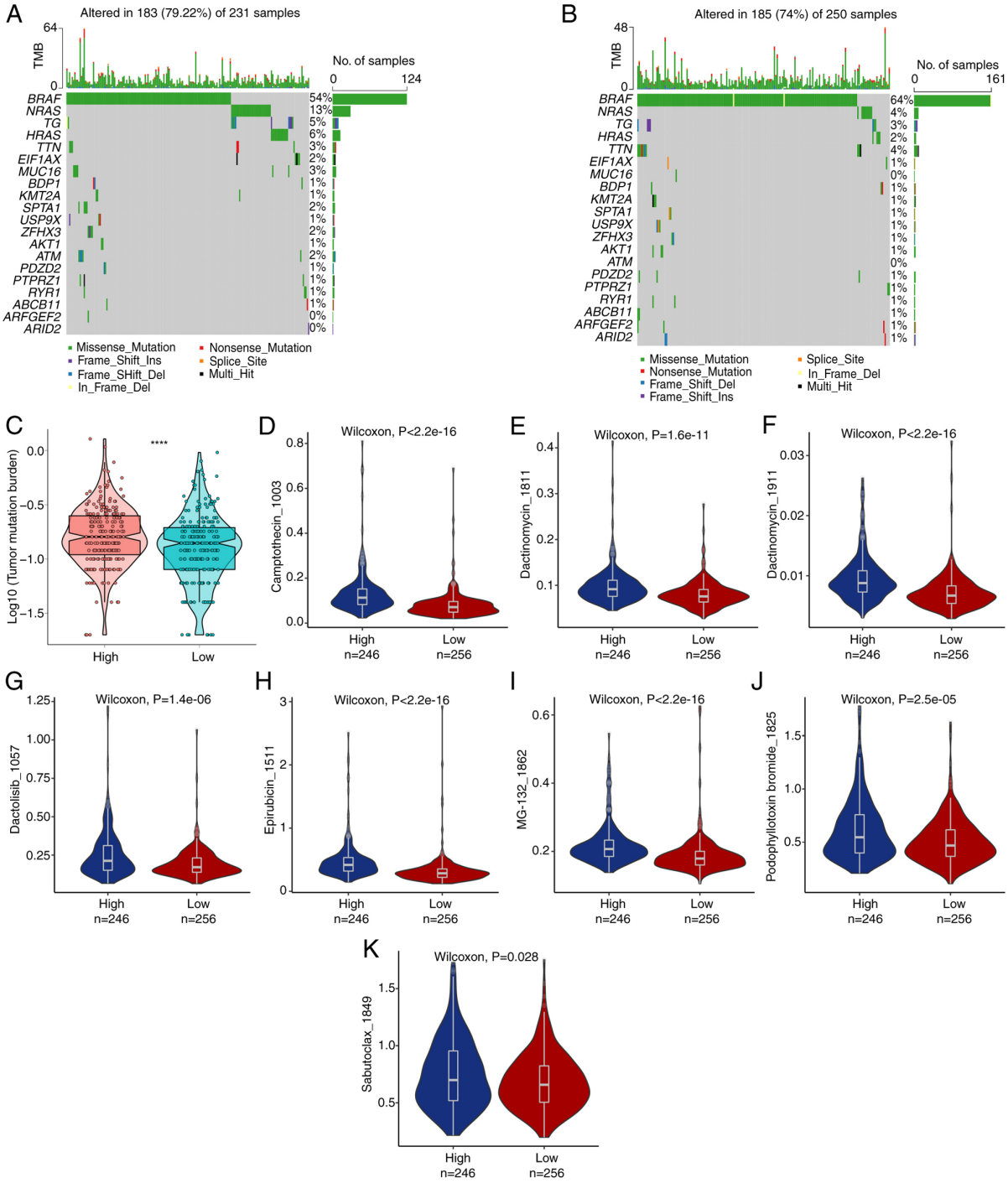

Figure 9. Discrepancy in TMB and drug susceptibility. Differences in TMB. The highest mutation frequency of the top 20 driver genes in the (A) high-risk group and (B) low-risk group. (C) Discrepancy in TMB between the two cohorts. (D) Discrepancy of Camptothecin_1003 among the two cohorts. (E) Difference of Dactinomycin_1811 between the two groups. (F) Discrepancy of Dactinomycin_1911 between the two cohorts. (G) Discrepancy of Dactolisib_1057 between the two groups. (H) Discrepancy of Epirubicin_1511 between the two cohorts. (I) Discrepancy of MG-132_1862 between the two groups. (J) Discrepancy of Podophyllotoxin bromide_1825 between the two cohorts. (K) Discrepancy of Sabutoclax_1849 between the two groups. ****P<0.0001. TMB, tumor mutation burden.

than 50% (Fig. 10B), followed by functional validation. After SIPA1L2 knockdown, EDU proliferation experiments detected enhanced proliferation ability in BCPAP and TPC-1 cell lines (Fig. 10C and D), scratch experiments detected enhanced migration ability in BCPAP and TPC-1 cell lines (Fig. 10E and F) and Transwell chamber experiments found enhanced invasion ability in BCPAP and TPC-1 cell lines (Fig. 10G and H). This indicated that SIPA1L2, as a protective gene, can inhibit the proliferation, migration and invasion abilities of TC cells.

Discussion

As immunotherapy continues to evolve, the importance of predictive biomarkers for response to immunotherapy is increasingly recognized (46,47). The effect of TME on the efficacy of cancer immunotherapy has been extensively studied and TME-related biomarkers are currently receiving increasing attention (48). However, reliable biomarkers and models that specifically target the impact of the TC TME on immunotherapy responses

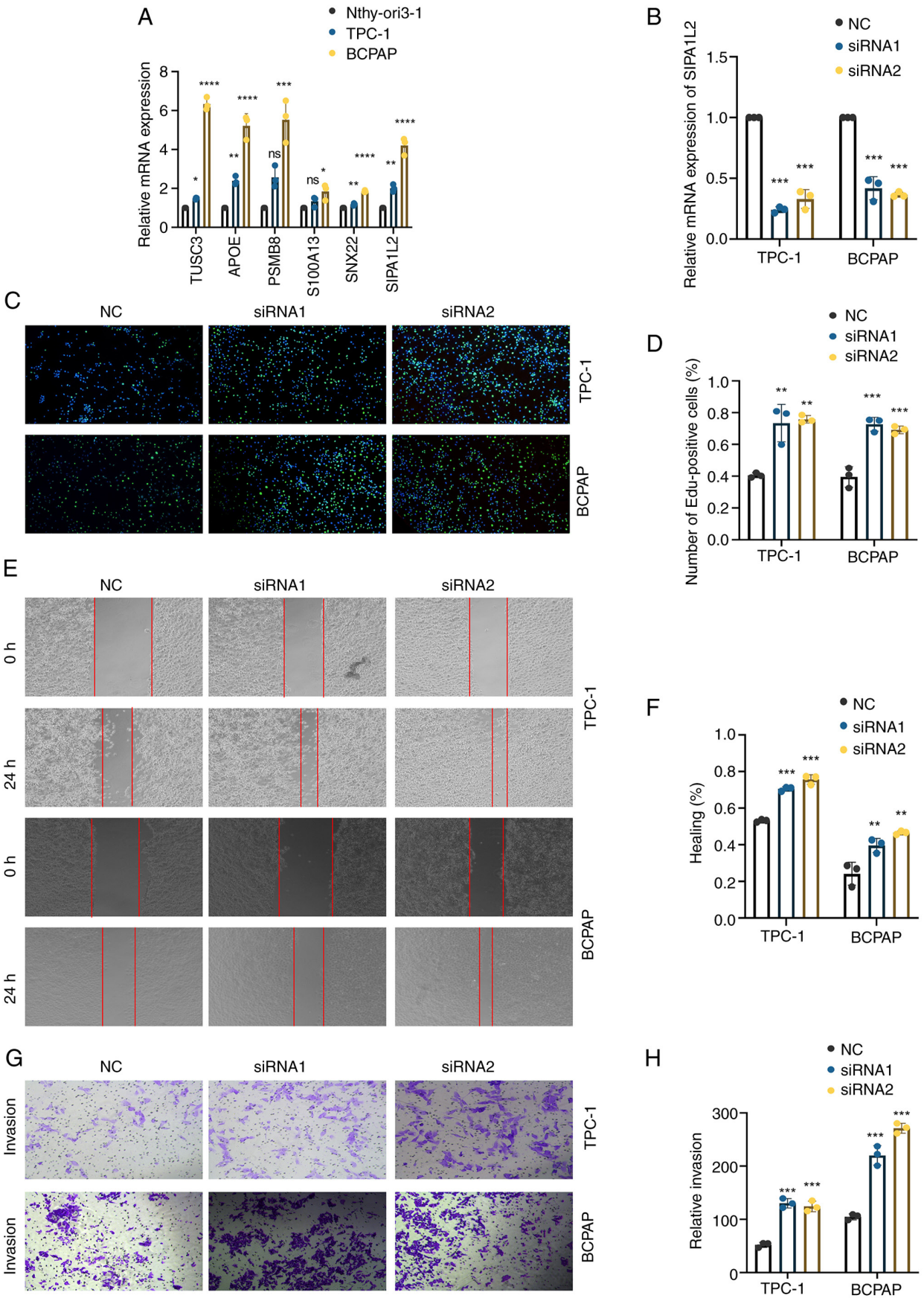

Figure 10. Expression of six genes in normal thyroid cells (Nthy-ori3-1) and TC cells (TPC-1, BCPAP), as well as the knockdown experiment of SIPA1L2 in TC cell lines. (A) mRNA levels of six genes in normal thyroid cells and TC cell lines. (B) Following SIPA1L2 knockdown, mRNA levels of TPC-1 and BCPAP cell lines. (C and D) The EdU proliferation assay showed that the proliferation ability of TPC-1 and BCPAP cell lines was enhanced after SIPA1L2 knockdown. (E and F) Wound healing experiments indicated that the migration ability of TPC-1 and BCPAP cell lines increased after SIPA1L2 knockdown. (G and H) Transwell assays demonstrated that the invasion ability of TPC-1 and BCPAP cell lines was enhanced after SIPA1L2 knockdown (*P<0.05, **P<0.01, ***P<0.001 and ****P<0.0001). TC, thyroid cancer; si, small interfering.

and prognosis remain limited. The continuous refinement of scRNA-seq technology has aided the thorough understanding of infiltrating immune cells in the TME. The present study analyzed seven TC samples using scRNA-seq and identified seven distinct cell types. The activity of glutamine metabolism-related genes was calculated using the AUCell algorithm, which revealed that these genes had the highest activity levels in epithelial cells. This result demonstrated that glutamine might regulate epithelial cells to influence TC progression. Pseudotime analysis indicated that the transition of epithelial cells from one state to another state during TC progression was related to metabolic and cell interactions. Further analysis uncovered the central roles of epithelial cells, macrophages and T cells in cellular communication, indicating the vital interaction between epithelial and immune cells for immune regulation and disease progression. Genes co-expressed in epithelial and TC cells were identified via the TCGA and GEO databases. Subsequent GO and KEGG analyses elucidated that epithelial cells might be instrumental in TC development through specific biological processes and pathways. Through Cox and Boruta feature selection techniques, six genes were pinpointed and used to establish a prognostic model. To ensure comprehensive validation and broad applicability of the prognostic markers, the present study established two cohorts (TCGA: training cohort and test cohort). A risk-scoring system was developed based on these six prognostic genes and cohorts were allocated to low- and high-risk subgroups. These markers consistently showed satisfactory performance in both cohorts, with worse outcomes in the high-risk subgroup, distinct variances in TME features between two subgroups and reliable accuracy for predicting 1-, 3- and 5-year OS.

GSEA and GSVA analyses of DEGs revealed that pathways such as lysine degradation, propionic acid metabolism and ascorbate and aldarate metabolism positively regulated TC progression, emphasizing the crucial role of metabolic programming in the TME. Among the six genes (S100A13, APOE, TUSC3, SNX22, SIPA1L2 and PSMB8) linked to these traits, APOE has been recognized as a predictive marker for immune infiltration in TC; FTO hinders glycolysis and TC progression by reducing APOE mRNA stability in an N6-methyladenosine-dependent manner (45,49). ZFPM1-AS1 transcription, mediated by STAT2, controls TC cell proliferation, movement and infiltration via the miR-515-5p/TUSC3 axis, where TUSC3 functions as an oncogene to enhance TC cell growth (44). miR-451a blocks epithelial-mesenchymal transition and triggers apoptosis in TC cells by targeting PSMB8 (50). S100A13 can promote TC progression in xenografted mouse models and HMGA1 enhances the proliferation and invasion of TC cells by upregulating S100A13 (51). These findings demonstrate the significant role of these four genes in TC progression. However, the involvement of SIPA1L2 in TC has not been studied. SIPA1, a member of the same family, is critical in the growth and metastasis of breast cancer (52). Additionally, research indicates that SNX22 could potentially be associated with radioresistance in nasopharyngeal cancer (53). Consistent with database analyses, these six genes showed mRNA expression differences in cell lines. Analysis of immune infiltration revealed varied immune cell populations, with a notable negative association between $CD8^+$ T cells and certain shared genes. This highlights the significance of epithelial and immune cell interactions in TC progression within the TME. Furthermore, the nomogram combining clinical features and risk scores could predict individualized survival for TC patients. In addition, drug sensitivity analysis uncovered that low-risk individuals might exhibit heightened responses to treatments involving Dactinomycin_1911 and MG-132_1862. Additionally, mRNA levels of these six genes were validated in two TC cell lines, largely consistent with database analyses. Based on existing literature and expression differences of the six genes, highly expressed SIPA1L2 in two TC cell lines was selected for knockdown experiments to study its role in TC cells. Following SIPA1L2 knockdown, the proliferation, migration and invasion abilities of TPC-1 and BCPAP cells were enhanced, indicating that SIPA1L2 may function as a tumor suppressor gene in these two TC cell lines. Although the present study was not able to collect clinical samples from hospitals to construct a prognostic model, the predictive model the present study was built using existing public databases can be used for subsequent prognostic predictions in patients with clinical TC. It is hoped to have the opportunity to conduct large-scale prospective clinical studies in the future to test the predictive importance of these prognostic features and to carry out further functional analysis and mechanism research.

Acknowledgements

Not applicable.

Funding

No funding was received.

Availability of data and materials

Data analyzed in the present study were sourced from GEO under GSE184362 and TCGA. The datasets generated in the present study may be requested from the corresponding author.

Authors' contributions

YiY, YHZ, ZLC and LCD participated in the study design, performed the preliminary analysis and drafted the article. YiY completed the experimental section. YPS, QW, WL and YX participated in data collection and literature review. FXT, HLD, YaY, JZ, YXG and YCL participated in data analysis. YH participated in study design, article revisions and provided experimental resources. YH, YiY and YHZ verified the authenticity of the raw data. All authors read and approved the final version of the manuscript.

Ethics approval and consent to participate

Not applicable.

Patient consent for publication

Not applicable.

Competing interests

The authors declare that they have no competing interests.

References

1. Carling T and Udelsman R: Thyroid cancer. Annu Rev Med 65: 125-137, 2014.
2. Laha D, Nilubol N and Boufraqech M: New therapies for advanced Thyroid cancer. Front Endocrinol (Lausanne) 11: 82, 2020.
3. Lim H, Devesa SS, Sosa JA, Check D and Kitahara CM: Trends in thyroid cancer incidence and mortality in the United States, 1974-2013. JAMA 317: 1338-1348, 2017.
4. Chen DW, Lang BHH, McLeod DSA, Newbold K and Haymart MR: Thyroid cancer. Lancet 401: 1531-1544, 2023.
5. Grimm D: Recent advances in thyroid cancer research. Int J Mol Sci 23: 4631, 2022.
6. Maniakas A, Dadu R, Busaidy NL, Wang JR, Ferrarotto R, Lu C, Williams MD, Gunn GB, Hofmann MC, Cote G, *et al*: Evaluation of overall survival in patients with anaplastic thyroid carcinoma, 2000-2019. JAMA Oncol 6: 1397-1404, 2020.
7. Araque KA, Gubbi S and Klubo-Gwiezdzinska J: Updates on the management of thyroid cancer. Horm Metab Res 52: 562-577, 2020.
8. Salgado SA, Kaye ER, Sargi Z, Chung CH and Papaleontiou M: Management of advanced thyroid cancer: Overview, advances, and opportunities. Am Soc Clin Oncol Educ Book 43: e389708, 2023.
9. Nakahara R, Maeda K, Aki S and Osawa T: Metabolic adaptations of cancer in extreme tumor microenvironments. Cancer Sci 114: 1200-1207, 2023.
10. Yang L, Venneti S and Nagrath D: Glutaminolysis: A hallmark of cancer metabolism. Annu Rev Biomed Eng 19: 163-194, 2017.
11. Li T and Le A: Glutamine metabolism in cancer. Adv Exp Med Biol 1063: 13-32, 2018.
12. Liu PS, Chen YT, Li X, Hsueh PC, Tzeng SF, Chen H, Shi PZ, Xie X, Parik S, Planque M, *et al*: CD40 signal rewires fatty acid and glutamine metabolism for stimulating macrophage anti-tumorigenic functions. Nat Immunol 24: 452-462, 2023.
13. Jin L, Alesi GN and Kang S: Glutaminolysis as a target for cancer therapy. Oncogene 35: 3619-3625, 2016.
14. Yu Y, Yu X, Fan C, Wang H, Wang R, Feng C and Guan H: Targeting glutaminase-mediated glutamine dependence in papillary thyroid cancer. J Mol Med (Berl) 96: 777-790, 2018.
15. Zhang GQ, Xi C, Ju NT, Shen CT, Qiu ZL, Song HJ and Luo QY: Targeting glutamine metabolism exhibits anti-tumor effects in thyroid cancer. J Endocrinol Invest 47: 1953-1969, 2024.
16. Chen S, Zhou Z, Li Y, Du Y and Chen G: Application of single-cell sequencing to the research of tumor microenvironment. Front Immunol 14: 1285540, 2023.
17. Ren X, Zhang L, Zhang Y, Li Z, Siemers N and Zhang Z: Insights gained from single-cell analysis of immune cells in the tumor microenvironment. Annu Rev Immunol 39: 583-609, 2021.
18. Liu L, Hou Y, Deng C, Tao Z, Chen Z, Hu J and Chen K: Single cell sequencing reveals that CD39 inhibition mediates changes to the tumor microenvironment. Nat Commun 13: 6740, 2022.
19. Hao X, Zheng Z, Liu H, Zhang Y, Kang J, Kong X, Rong D, Sun G, Sun G, Liu L, *et al*: Inhibition of APOC1 promotes the transformation of M2 into M1 macrophages via the ferroptosis pathway and enhances anti-PD1 immunotherapy in hepatocellular carcinoma based on single-cell RNA sequencing. Redox Biol 56: 102463, 2022.
20. Colaprico A, Silva TC, Olsen C, Garofano L, Cava C, Garolini D, Sabedot TS, Malta TM, Pagnotta SM, Castiglioni I, *et al*: TCGAbiolinks: An R/Bioconductor package for integrative analysis of TCGA data. Nucleic Acids Res 44: e71, 2016.
21. Butler A, Hoffman P, Smibert P, Papalexi E and Satija R: Integrating single-cell transcriptomic data across different conditions, technologies, and species. Nat Biotechnol 36: 411-420, 2018.
22. Van de Sande B, Flerin C, Davie K, De Waegeneer M, Hulselmans G, Aibar S, Seurinck R, Saelens W, Cannoodt R, Rouchon Q, *et al*: A scalable SCENIC workflow for single-cell gene regulatory network analysis. Nat Protoc 15: 2247-2276, 2020.
23. Qiu X, Mao Q, Tang Y, Wang L, Chawla R, Pliner HA and Trapnell C: Reversed graph embedding resolves complex single-cell trajectories. Nat Methods 14: 979-982, 2017.
24. Karmaus PWF, Chen X, Lim SA, Herrada AA, Nguyen TM, Xu B, Dhungana Y, Rankin S, Chen W, Rosencrance C, *et al*: Metabolic heterogeneity underlies reciprocal fates of T(H)17 cell stemness and plasticity. Nature 565: 101-105, 2019.
25. Armingol E, Officer A, Harismendy O and Lewis NE: Deciphering cell-cell interactions and communication from gene expression. Nat Rev Genet 22: 71-88, 2021.
26. Fang Z, Tian Y, Sui C, Guo Y, Hu X, Lai Y, Liao Z, Li J, Feng G, Jin L and Qian K: Single-Cell transcriptomics of proliferative phase endometrium: Systems analysis of cell-cell communication network using CellChat. Front Cell Dev Biol 10: 919731, 2022.
27. Gene Ontology Consortium: Gene ontology consortium: Going forward. Nucleic Acids Res 43: D1049-D1056, 2015.
28. Kanehisa M and Goto S: KEGG: Kyoto encyclopedia of genes and genomes. Nucleic Acids Res 28: 27-30, 2000.
29. Yu G, Wang LG, Han Y and He QY: clusterProfiler: An R package for comparing biological themes among gene clusters. OMICS 16: 284-287, 2012.
30. Ye Z, An S, Gao Y, Xie E, Zhao X, Guo Z, Li Y, Shen N, Ren J and Zheng J: The prediction of in-hospital mortality in chronic kidney disease patients with coronary artery disease using machine learning models. Eur J Med Res 28: 33, 2023.
31. Subramanian A, Tamayo P, Mootha VK, Mukherjee S, Ebert BL, Gillette MA, Paulovich A, Pomeroy SL, Golub TR, Lander ES and Mesirov JP: Gene set enrichment analysis: A knowledge-based approach for interpreting genome-wide expression profiles. Proc Natl Acad Sci USA 102: 15545-15550, 2005.
32. Ritchie ME, Phipson B, Wu D, Hu Y, Law CW, Shi W and Smyth GK: limma powers differential expression analyses for RNA-sequencing and microarray studies. Nucleic Acids Res 43: e47, 2015.
33. Liberzon A, Subramanian A, Pinchback R, Thorvaldsdóttir H, Tamayo P and Mesirov JP: Molecular signatures database (MSigDB) 3.0. Bioinformatics 27: 1739-1740, 2011.
34. Liberzon A, Birger C, Thorvaldsdóttir H, Ghandi M, Mesirov JP and Tamayo P: The molecular signatures database (MSigDB) hallmark gene set collection. Cell Syst 1: 417-425, 2015.
35. Fan X, Chen H, Jiang F, Xu C, Wang Y, Wang H, Li M, Wei W, Song J, Zhong D and Li G: Comprehensive analysis of cuproptosis-related genes in immune infiltration in ischemic stroke. Front Neurol 13: 1077178, 2022.
36. Wu S, Lv X, Li Y, Gao X, Ma Z, Fu X and Li Y: Integrated Machine learning and single-sample gene set enrichment analysis identifies a TGF-beta signaling pathway derived score in headneck squamous cell carcinoma. J Oncol 2022: 3140263, 2022.
37. Ru B, Wong CN, Tong Y, Zhong JY, Zhong SSW, Wu WC, Chu KC, Wong CY, Lau CY, Chen I, *et al*: TISIDB: An integrated repository portal for tumor-immune system interactions. Bioinformatics 35: 4200-4202, 2019.
38. Ito K and Murphy D: Application of ggplot2 to pharmacometric graphics. CPT Pharmacometrics Syst Pharmacol 2: e79, 2013.
39. Maeser D, Gruener RF and Huang RS: oncoPredict: An R package for predicting in vivo or cancer patient drug response and biomarkers from cell line screening data. Brief Bioinform 22: bbab260, 2021.
40. Yang W, Soares J, Greninger P, Edelman EJ, Lightfoot H, Forbes S, Bindal N, Beare D, Smith JA, Thompson IR, *et al*: Genomics of drug sensitivity in cancer (GDSC): A resource for therapeutic biomarker discovery in cancer cells. Nucleic Acids Res 41: D955-D961, 2013.
41. Mayakonda A, Lin DC, Assenov Y, Plass C and Koeffler HP: Maftools: Efficient and comprehensive analysis of somatic variants in cancer. Genome Res 28: 1747-1756, 2018.
42. Liu Z, Wang L, Guo C, Liu L, Jiao D, Sun Z, Wu K, Zhao Y and Han X: TTN/OBSCN 'Double-Hit' predicts favourable prognosis, 'immune-hot' subtype and potentially better immunotherapeutic efficacy in colorectal cancer. J Cell Mol Med 25: 3239-3251, 2021.
43. Schmittgen TD and Livak KJ: Analyzing real-time PCR data by the comparative C(T) method. Nat Protoc 3: 1101-1108, 2008.
44. Ren R, Du Y, Niu X and Zang R: ZFPM2-AS1 transcriptionally mediated by STAT1 regulates thyroid cancer cell growth, migration and invasion via miR-515-5p/TUSC3. J Cancer 12: 3393-3406, 2021.
45. Lin X, Zhang J, Zhao RH, Zhang WJ, Wu JF and Xue G: APOE is a prognostic biomarker and correlates with immune infiltrates in papillary thyroid carcinoma. J Cancer 13: 1652-1663, 2022.
46. Zhu H, Tang K, Chen G and Liu Z: Biomarkers in oral immunotherapy. J Zhejiang Univ Sci B 23: 705-731, 2022.
47. Mino-Kenudson M, Schalper K, Cooper W, Dacic S, Hirsch FR, Jain D, Lopez-Rios F, Tsao MS, Yatabe Y, Beasley MB, *et al*: Predictive biomarkers for immunotherapy in lung cancer: Perspective from the international association for the study of lung cancer pathology committee. J Thorac Oncol 17: 1335-1354, 2022.

48. Liu Y, Xun Z, Ma K, Liang S, Li X, Zhou S, Sun L, Liu Y, Du Y, Guo X, *et al*: Identification of a tumour immune barrier in the HCC microenvironment that determines the efficacy of immunotherapy. J Hepatol 78: 770-782, 2023.
49. Huang J, Sun W, Wang Z, Lv C, Zhang T, Zhang D, Dong W, Shao L, He L, Ji X, *et al*: FTO suppresses glycolysis and growth of papillary thyroid cancer via decreasing stability of APOE mRNA in an N6-methyladenosine-dependent manner. J Exp Clin Cancer Res 41: 42, 2022.
50. Fan X and Zhao Y: miR-451a inhibits cancer growth, epithelial-mesenchymal transition and induces apoptosis in papillary thyroid cancer by targeting PSMB8. J Cell Mol Med 23: 8067-8075, 2019.
51. Zhong J, Liu C, Chen YJ, Zhang QH, Yang J, Kang X, Chen SR, Wen GB, Zu XY and Cao RX: The association between S100A13 and HMGA1 in the modulation of thyroid cancer proliferation and invasion. J Transl Med 14: 80, 2016.
52. Liu C, Jiang WG, Hargest R and Martin TA: The role of SIPA1 in the development of cancer and metastases (Review). Mol Clin Oncol 13: 32, 2020.
53. Zhou Z, Chen G, Shen M, Li J, Liu K, Liu M, Shi S, Yang D, Chen W, Chen S, *et al*: Genome-scale CRISPR-Cas9 knockout screening in nasopharyngeal carcinoma for radiosensitive and radioresistant genes. Transl Oncol 30: 101625, 2023.

Copyright © 2025 You et al. This work is licensed under a Creative Commons Attribution-NonCommercial-NoDerivatives 4.0 International (CC BY-NC-ND 4.0) License.